# Observation of Individual Dislocations in 6H and 4H SiC by Means of Back-Reflection Methods of X-Ray Diffraction Topography

W.Wierzchowski[1*)], K.Wieteska[2)], T. Balcer[1)], A.Malinowska[1), 3)]
W.Graeff[4)], W. Hofman[1)]

[1)] *Institute of Electronic Materials Technology, ul. Wólczyńska 133, 01-919 Warsaw, Poland*

[2)] *Institute of Atomic Energy, 05-400 Otwock-Świerk, Poland*

[3)] *Faculty of Physics Warsaw University of Technology, ul. Koszykowa 75, 00-662 Warsaw, Poland*

[4)] *HASYLAB at DESY, Notkestr.85, 22603 Hamburg, Germany*

Keywords: silicon carbide, X-ray diffraction topography, dislocations
PACS number: 61.72.Ff

## Abstract

SiC crystals of high structural perfection were investigated with several methods of X-ray diffraction topography in Bragg-case geometry. The methods included section and projection synchrotron white beam topography and monochromatic beam topography. The investigated 6H and 4H samples contained in large regions dislocations of density not exceeding $10^3$ $cm^{-2}$. Most of them cannot be interpreted as hollow core dislocations (micro- or nanopipes). The concentration of the latter was lower than $10^2$ $cm^{-2}$. The present investigation confirmed the possibility of revealing dislocations with all used methods. The quality of presently obtained Bragg-case multi-crystal and section images of dislocation enabled analysis based on comparison with numerically simulated images. The analysis confirmed the domination of screw-type dislocations in the investigated crystals.

* corresponding author, phone (4822) 8353041 ex. 496, fax (4822) 8349003,
e-mail address wierzc_w@itme.edu .pl

## 1. Introduction

Growth of SiC crystals and epitaxial layers is widely developed for present and future applications in technology of high temperature electronic devices and blue light optoelectronic elements [1-3]. The effective tool of improving the required crystallographic perfection of SiC are X-ray topographic investigations [4-10]. The topographic conventional and synchrotron experiments supported by numerical simulation of the images, were applied by Dudley and his coworkers [6-9] for studying so called nano-, micro- and macro-pipes being a very important problem in the application of SiC. The results support the interpretation of micro- and nano-pipes as super screw dislocations formed jointly by many screw dislocations.

In the topographic investigation the Bragg-case geometry is less popular than the transmission geometry. However, it can be often very useful providing more transparent images at higher concentration of defects.

In the present work we investigated SiC crystals of high structural perfection with several methods of X-ray diffraction topography in Bragg-case geometry using synchrotron radiations. For simulation we applied numerical programmes described in [11-13]

## 2. Experimental.

The experimental Bragg-case images were obtained at HASYLAB using X- ray beam from the DORIS-III storage ring. The monochromatic beam (multi-crystal) diffraction topographs were obtained at the experimental station E2 using 0.1115 nm radiation monochromatised by successive 511 and 333 reflections from silicon crystals. In the case of 6H sample the topographs were obtained with 00·12 reflection, and for 4H with 00·4

reflection. In addition to monochromatic beam topographs, the local rocking curves were recorded using a probe beam with a diameter 50 μm.

The white beam projection and section images were exposed at the experimental station F 2 using the slits which enabled to limit the beam front to the width smaller than 5μ m. The investigated crystals were inclined at a small glancing angles $5^o$ and $10^o$ about the axis perpendicular to the beam. Similarly as in the case of Laue method, a single exposure provided a number of spots corresponding to different reflections. The majority of the spots corresponded to the "skew" reflections, when the plane of diffraction does not contain the normal to crystal surface, but for simulations more suitable were so called "zero layer" reflections.

For the present investigation we chose the most perfect crystals available. The investigated samples were 6H and 4H wafers manufactured by Cree Inc. which contained in some regions the dislocation density on the level not exceeding $10^3$ $cm^{-2}$ which could not be interpreted as hollow core dislocations (micro- or nano-pipes). The concentration of the latter was evaluated by polariscopic microscopy as not exceeding $10^2$ $cm^{-2}$

## 3. Numerical simulation

The present simulations were realised with slightly modified programs used previously for performing the simulations described by Wierzchowski et al. [11-13] The algorithms both with constant and variable step of integration were used. The integration grids corresponding to the present cases are shown in figure 1.

**Fig. 1.** Integration grids used for present numerical simulations (**a) –**for monochromatic beam (multi-crystal) topography, and (**b)** – for Bragg-case section topography.

It may be noted that the development of the computer technique enables effective image simulation with modern personal computers and the use of variable step is not essential. In some simulations we also took into account the divergence of the incident beam by adding simulations for incident plane waves with limited wave front and glancing angles stepwise changed by an appropriate small angle. Good quality images were obtained adding 100 or more simulations, both in the case of multi-crystal and section topography, corresponding to a plane wave with the angle of incidence stepwise changed in a range of 10-20".

In all simulations the form of Takagi-Taupin equations proposed by Bedyńska [14] was used. The procedures used for calculation of the contribution of the displacement field for oblique dislocations were written basing on the paper by Shaibani and Hazzledine [15]

## 4. Results and discussion

The chosen 6H sample contained also some area with relatively large concentration of defects. It is illustrated in particular by Fig. 2 presenting white beam and optical polariscopic images of the region containing some micro-pipes and large concentration of defects.

**Fig. 2. (a)** White beam topographic image of the region of SiC sample surrounding some micro-pipes with a considerable density of dislocations.
**(b)** Polariscopic image of the micro pipes in the same sample .

Next, in Fig. 3 a, b we present the monochromatic beam topographs obtained with 00·12 reflection of 0.1115 nm of a larger part of this sample with two different regions, significantly differing in crystallographic perfection. In one region close to some micro-pipes one can notice that the images form some narrow irregular stripes, which become much wider in

another, much more perfect region. The two topographs were taken at two angular settings differing by 0.001°, resulting in different location of the stripe. A larger magnification of a highly perfect region, providing characteristic images of dislocations is shown in Fig. 3 c and d, with some residual fragments of a rosette and a larger tail coming from the dislocation core. The FWHM of the rocking curve recorded with a 50 μm probe beam was only 4.5 “.

**Fig. 3 (a, b) -**Monochromatic beam topographs of 6 H sample taken with 00·12 reflection of 0.1115 nm of a larger part of the sample with regions differing in crystallographic perfection, taken at two angular settings differing by 0.001° , **c, d.** enlarged fragments of **a, b** with low dislocation density.

**Fig. 4** Monochromatic beam topographs of 4 H samples taken with 00·4 reflection of 0.1115 nm with low dislocation density.

**Fig. 5 (a, b)** Simulated monochromatic beam topographs for two different signs of the Burgers vector for the low-angle flank of the rocking curve. The topograph **(a)** corresponds to the Burgers Vector $[00\cdot\bar{1}]$ and **(b)** to $[00\cdot 1]$ respectively. The simulated images are similar to those observed at the right side of topograph shown in Fig. 5.

These features of a dislocation images are even more clearly visible in monochromatic beam topographs of 4H samples in asymmetric (due to 9° off-cut) 00·4 reflection shown in Fig. 4 . In the topograph we observe mainly two types of rosettes, one of them seemingly of reversed contrast with respect to the other. This type of images is similar to the one discussed by Bedyńska [14] for the screw dislocations, which is also the expected dominant type of dislocations in SiC crystals.

It is confirmed by actually performed simulations for two orientation of Burgers vector at the low-angle flank of the rocking curve, shown in Fig. 5. The simulated images

exhibit reasonable similarity to the experimental images despite many possible discrepancy factors connected with the imperfection of the crystal. In particular these imperfections seem to be a possible reason of the significant dampening of the interferences due to the dislocation core, which are present in the theoretical images.

In the case of white beam synchrotron topography the dislocation are well resolved only in part reflections. In that case projection topographs provide the images of dislocation in the form of characteristic dots and commas, as it may be seen in Fig. 6a.

**Fig. 6 (a)** Back-reflection white beam projection synchrotron topographs of the 4 H wafer shown in Fig. 5a with low density of dislocations, forming the images of dislocations in form of "dots".
**(b)** The enlarged fragment of the back reflection white beam section synchrotron topographs of the 4 H wafer shown in Fig. 5a with low density of dislocations, forming the images of dislocations in form of "black rosettes".

Despite the curvature of the sample, the Bragg-case section images reproduce the images of dislocations in form of black rosettes (Fig. 6b). It was possible to obtain similar character of the dislocation images in the simulated section topographs, in Fig. 7 also assuming a screw type of dislocations.

**Fig 7.** The numerically simulated white beam back reflection section multi-crystal images of screw dislocation analogous to seen in Fig. 6b.

In the section topographs the interference fringes connected with curvature and strain gradients could be expected to dampen out. In this technique the image is due mainly to strain gradient in the region where the beam intersects the dislocation [13] as in our simulation done for dislocation in a perfect crystal (Fig. 7).

## Conclusions

The present investigation confirmed the possibility of revealing dislocations with all used methods. The character of the images was significantly different in the case of different topographic methods. The images of dislocation in synchrotron and conventional multi-crystal arrangement consisted of characteristic rosettes with a “tail” coming from the dislocation core, while single crystal projection topographs provided the images of dislocation in the form of characteristic dots or commas and section images reproduced the dislocations in form of black rosettes.

The quality of presently obtained Bragg-case multi-crystal and section images of dislocation enabled analysis based on comparison with numerically simulated images. The analysis confirmed the domination of screw-type dislocations in the investigated crystals.

**Acknowledgement**

The present work was supported by the State Committee for Scientific Research (grant 3 T10C 022 29).

**References:**

[1] H. Morkoç, S. S. Strite, S. Gao, G.B. Lin, B. Sverdlov, M. Burns, J. Appl. Phys. **76,** 1363 (1994).

[2] B. Hobgood, M. Brady, W. Brixius, G. Fechko, R. Glass, D. Henshall, J. Jenny, R. Leonard, D. Malta, St.G. Mueller, V. Tsvetkov, C. Carter Jr.: Material Sci. Forum,

**338-342,** 3 (2000).

[3] A.S. Bakin, S.I. Dorozhin: IEEE Conference Series **98 EX132** , 2 (1998).

[4] E. Pernot, P. Pernot-Rejmánková, M Anikin, B. Pellisier, C. Moulin and R. Madar, J. Phys. D: Appl. Phys. **34,** A136 (2001).

[5] A.R. Lang, A.P.W. Makepeace, J. Phys. D. Appl. Phys. **32,** A97 (1999).

[6] M. Dudley X.R. Huang, V.M. Vetter, J. Phys. D. Appl. Phys. **36,** A30 (2003).

[7] X.R. Huang, M. Dudley. W.M. Vetter, W. Huang, W. Si, C.H. Carter, J. Appl. Cryst. **32,** 516 (1999).

[8] W.M. Vetter, M. Dudley, J. Appl. Cryst. **42,** 2157 (1998).

[9] J. Härtwig, J. Baruchel, H. Kuhn, X.-Huang, M. Dudley, E. Pernot, Nucl. Inst. Methods in Phys. Res. B **200**, 323 (2003).

[10] R. Yakimova, M. Syväjärvi, H. Jacobson, E. Janzén, in: Recent Research Development in Materials and Engineering, Eds. J.J. Moore, G.G. Richards and H.Y. Sohn, Transworld Research Network, Kerala 2002, p. 619

[11] W. Wierzchowski, phys. stat. sol. (a) **88**, 77 (1985).

[12] W. Wierzchowski, K. Mazur, K. Wieteska, J. Phys. D. **28** A33 (1995).

[13] W.K. Wierzchowski, K. Wieteska, W. Graeff, J. Phys. D. **33**, 1230 (2000).

[14] T. Bedynska, Phys Stat. Sol. (a), **18**, 147 (1973).

[15] S.J. Shaibani, P.M. Hazzledine, Phil. Mag. A **44**, 657 (1981).

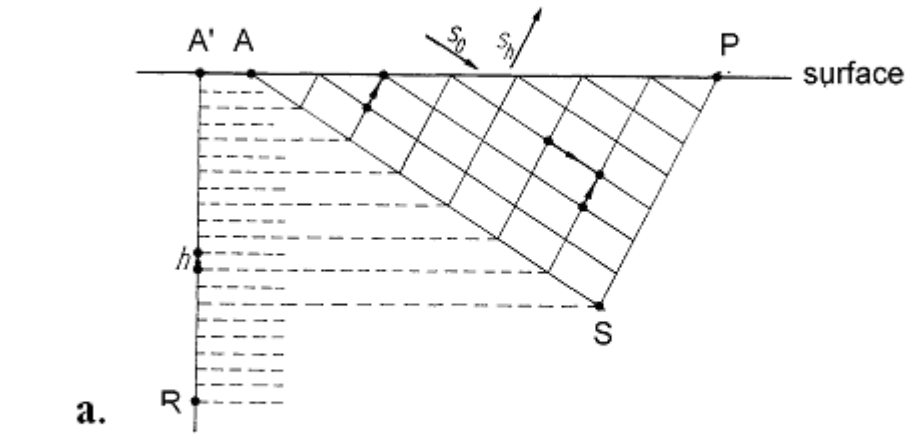


a.

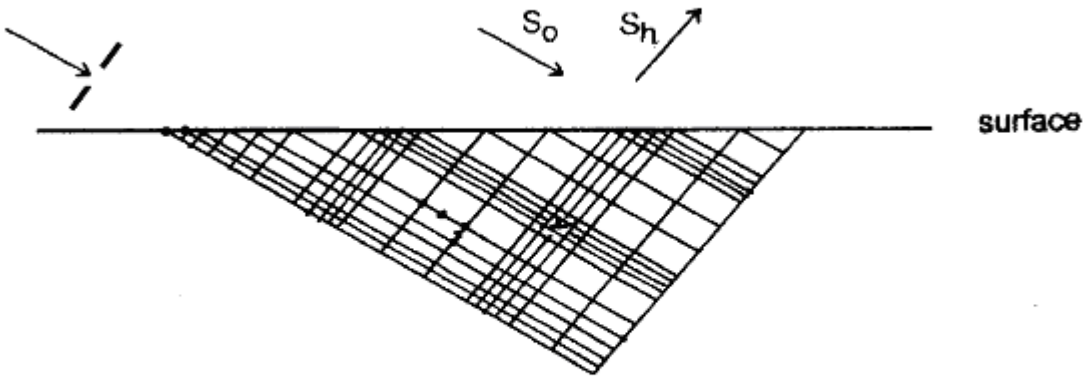


b.

**Fig. 1.**

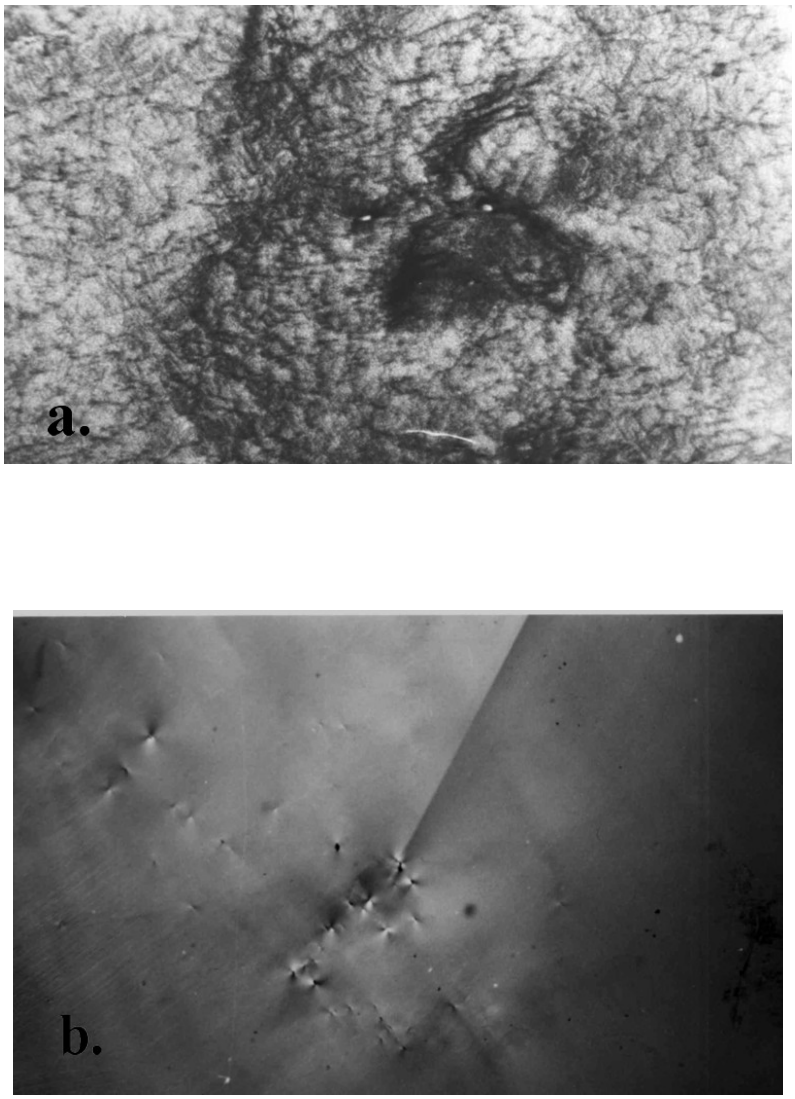


**Fig. 2**

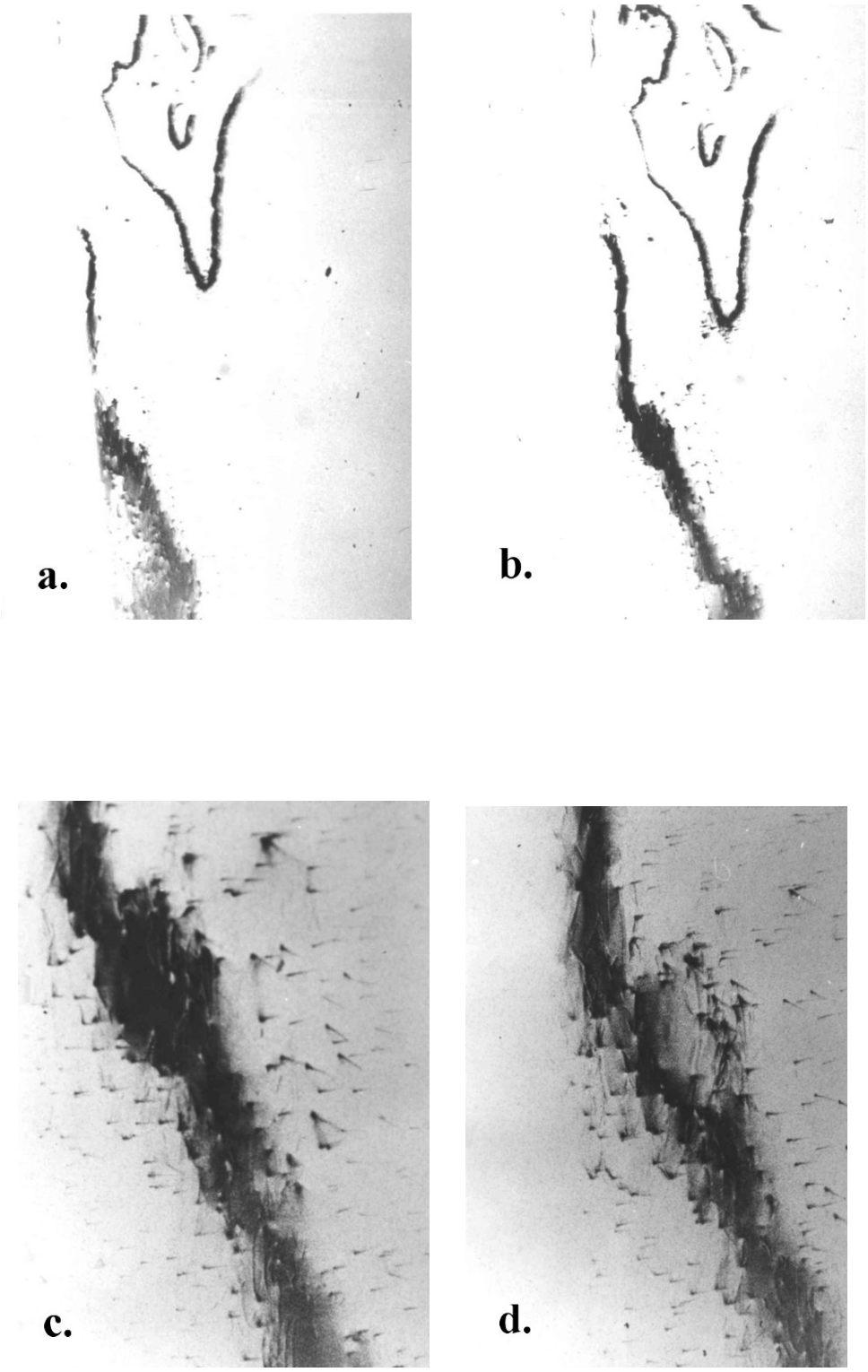


**Fig. 3.**

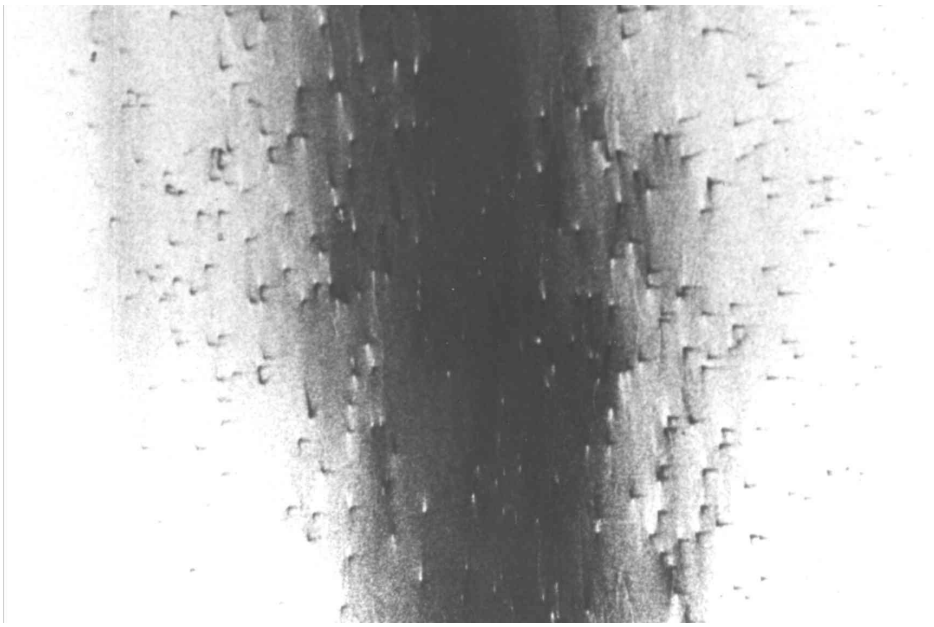

a.
a.

**Fig. 4**

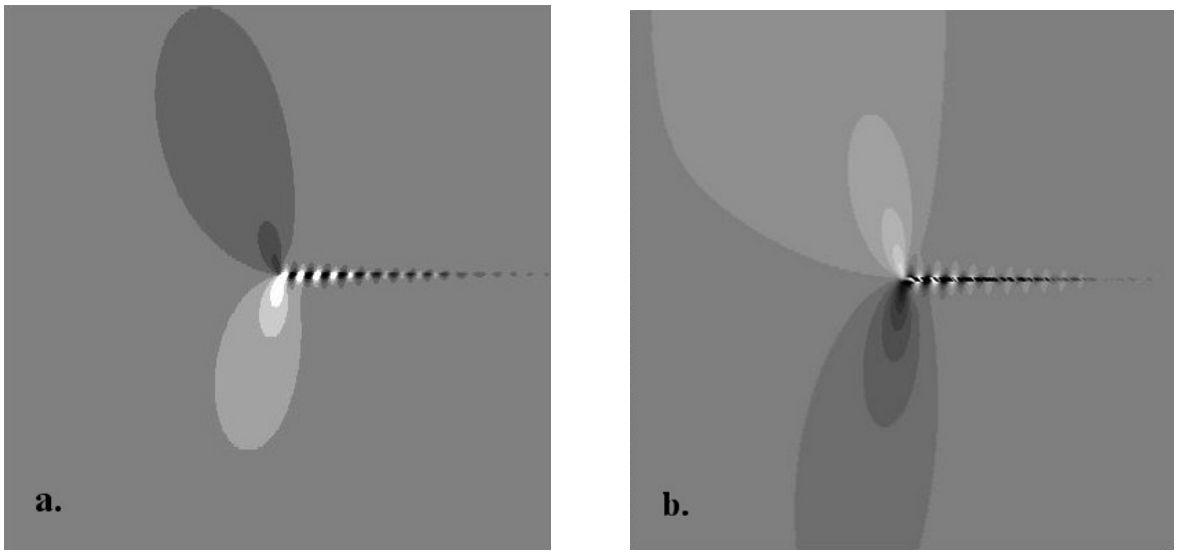


**Fig. 5**

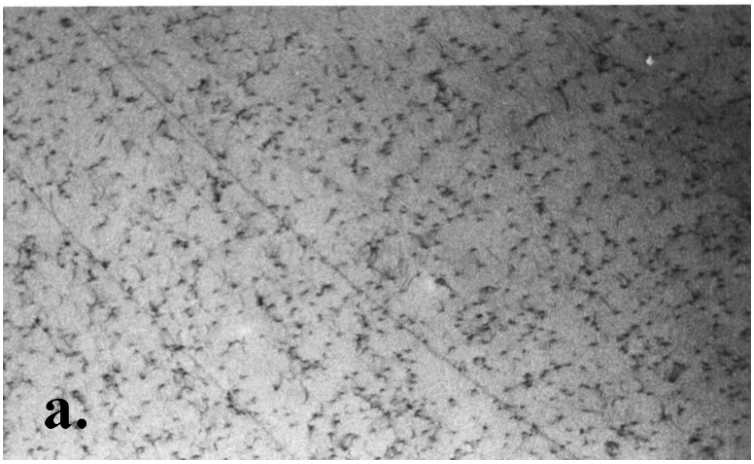


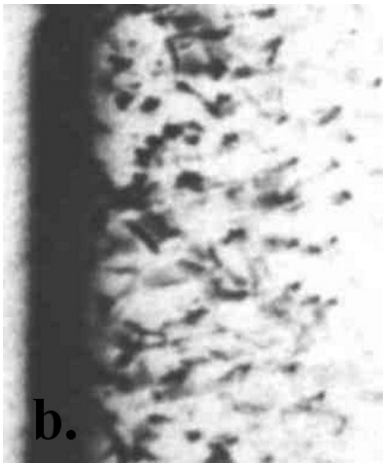


**Fig. 6**

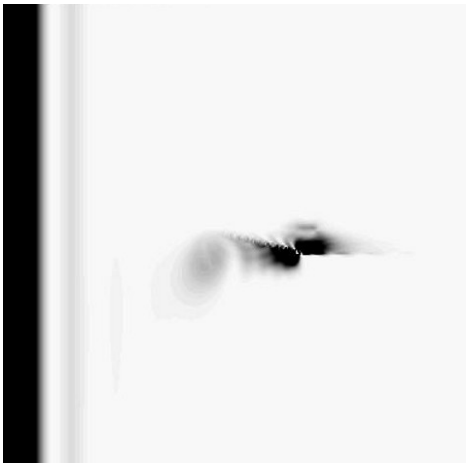

**Fig 7.**